Influence of Magnet Shape on the Cogging Torque of a Surface-mounted Permanent Magnet Motor*

Min Zhou[1, 2], *Xinxing Zhang*[3*], *Wenxiang Zhao*[2], *Jinghua Ji*[2] *and Jingning Hu*[1]

(1. Research Center of Fluid Machinery Engineering and Technology, Jiangsu University, Zhenjiang 212013, China;
2. School of Electrical and Information Engineering, Jiangsu University, Zhenjiang 212013, China;
3. Jingjiang College, Jiangsu University, Zhenjiang 212013, China)

Abstract: The influence of bread-loaf shaped magnet poles under parallel magnetization on the cogging torque of surface-mounted permanent magnet (SPM) motors is studied. For the SPM motors having magnetic poles with eccentricity and sine harmonic compensation, the electromagnetic performances of integer and fractional slot motors are compared. It is found that the cogging torque and torque ripple of the integer and fractional slot motors can be reduced with the same eccentric magnet pole. The cogging torque and torque ripple of a fractional slot motor can be decreased by sine harmonic compensation, however, the same sine harmonic compensation has a small influence in integer slot motors. By varying the magnetic poles, the contribution of the field harmonics ($k = (2n + 1)\ p$), which are a direct result of magnet magnetization, to the cogging torque also changes. The electromagnetic performance of a 3 kW prototype is tested, and it is found that the experimental results validate the theoretical investigation.

Keywords: Analytical model, bread-loaf magnet shape, finite-element (FE), cogging torque, surface-mounted permanent magnet (SPM) motor

1 Introduction

The surface-mounted permanent magnet (SPM) motor has many advantages, such as a small size, light weight, simple structure, reliable operation, and high torque density. It is widely used in ship construction, aviation, public life, and other fields[1-5]. However, the interaction between the permanent magnet (PM) and stator slot can lead to a cogging torque, which has a great influence on the torque ripple and affects the entire performance of the motor. To minimize the cogging torque, many methods have been studied. In particular, skewing of the stator slots has been widely used to reduce cogging torque[6-7]. However, the skewing of stator slots is difficult and can therefore increase production costs. Additionally, the eccentric structure of the teeth was proposed to replace the skewing technique[8]. Moreover, unequal teeth widths were designed to reduce low-order cogging torque harmonics[9-10]. Furthermore, changing the slot openings and position or rotor shape were also proposed to reduce the cogging torque[11-13].

In particular, the cogging torque can be effectively weakened by changing the shape of the magnet poles[14-16]. The cogging torque can be directly calculated by the finite-element (FE) method. In Ref. [17], the cogging torque was calculated based on the FE method, which is highly flexible. It has an outstanding ability to analyze complex systems and to consider saturation effects. In Ref. [18], the FE method is widely used to evaluate the effect of optimizing the magnetic pole shape on the cogging torque, but it does not sufficiently reveal the source of the cogging torque. Although the energy method and the accurate subdomain model can accurately predict the cogging torque[19-21], none of these analytical models consider the effect of different magnet pole shapes. Although the cogging torque due to eccentric magnet poles can be predicted[19-23], the prediction process is very complicated. In Ref. [24], a tangent harmonic compensation (THC) method for optimizing the magnet shape of a 6-pole/9-slot motor was presented. It adapts to cases in which low torque ripples are obtained. It investigated the influence of magnet shape on the cogging torque of motors. Furthermore, the sensitivity of the cogging torque to the magnet shape between the integer slot and fractional slot motors was

* Corresponding Author, Email: zhangxinxing@ujs.edu.cn
* Supported by the Key Research and Development Program of Jiangsu Province (BE2018107).
Digital Object Identifier: 10.23919/CJEE.2019.000026

compared.

In this paper, the FE and analytical methods will be presented based on the Maxwell stress tensor. The analytical method is based on Zhu [21]. The goal of the hybrid FE and analytical method is to reflect the effect of the shape of the magnet poles on the cogging torque qualitatively. After the shape of the magnet poles was changed, to better analyze the variation in each field harmonic, the FE and analytical method is adopted. In Section 2, the analysis method is briefly introduced. Subsequently, the different magnet pole shapes are presented in Section 3. In Section 4, simulation results are given to explain the source of the cogging torque, and the torque performance of the integer and fractional slot motors are compared. Moreover, a 12-pole/36-slot prototype with eccentric magnet poles is assessed experimentally to validate the theoretical analysis. Finally, conclusions are drawn in Section 5.

2 Analysis method

Fig. 1 shows that the subdomain model. As can be seen, the inner and outer radii of PM are expressed by R_r and R_m, respectively. R_s is the inner radius of the stator, and R_{sb} is the radius of the slot bottom. Furthermore, R_m varies with position.

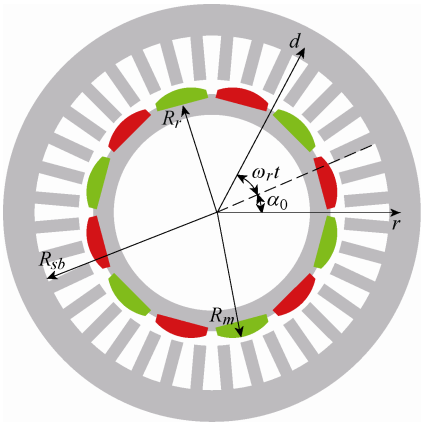

Fig. 1 Subdomain model

The radial and tangential components of the air-gap flux density can be obtained as [21]

$$B_{rg}=\sum_k B_{rck}\cos k\alpha+\sum_k B_{rsk}\sin k\alpha \tag{1}$$

$$B_{\alpha g}=\sum_k B_{\alpha ck}\cos k\alpha+\sum_k B_{\alpha sk}\sin k\alpha \tag{2}$$

where B_{rck}, B_{rsk}, $B_{\alpha ck}$, and $B_{\alpha sk}$ are the k-th harmonic amplitudes corresponding to B_{rg} and $B_{\alpha g}$. The details of their calculation are given in Ref. [21].

The harmonic amplitudes B_{rck} can be expressed as [21]

$$B_{rck}=A_{4k}\cos\left(k\omega_r t+k\alpha_0\right)\left[\gamma(k)M_{rk}+\zeta(k)M_{\alpha k}\right]f_{Br}-g_{Br}\sum_i\sum_m C_{ei}(m)\eta_{si}(m,k) \tag{3}$$

where ω_r is the rotor rotational speed, α_0 is the rotor initial position, k and m are harmonic orders, the A_{4k}, γ, ζ, f_{Br}, g_{Br}, C_{ei}, η, M_{rk}, and $M_{\alpha k}$ are as given in Ref. [21].

According to formula (3), the value of B_{rck} is related to M_{rk} and $M_{\alpha k}$, variables related to the magnetization of magnets. For parallel magnetization, M_{rk} and $M_{\alpha k}$ can be expressed as

$$M_{rk}=\begin{cases}\dfrac{B_r}{\mu_0}\alpha_p(A_{1k}+A_{2k}) & k/p=1,3,5,\cdots\\ 0 & \text{others}\end{cases} \tag{4}$$

$$M_{\alpha k}=\begin{cases}\dfrac{B_r}{\mu_0}\alpha_p(A_{1k}-A_{2k}) & k/p=1,3,5,\cdots\\ 0 & \text{others}\end{cases} \tag{5}$$

where μ_0 is the relative permeability of air, B_r is residual flux density of a magnet, and α_p is the pole-arc to pole-pitch ratio, p is the number of pole pairs, the A_{1k} and A_{2k} are as given in Ref. [21]. According to formulas (4)-(5) when $k\neq(2n+1)p$ (n= 0, 1, 2, ⋯), the value of B_{rck} is zero. Similarly, the value of B_{rsk}, $B_{\alpha ck}$, B_{rck}, and $B_{\alpha sk}$ are zero.

Based on Maxwell tensor method, the expression of the cogging torque can be obtained by the air-gap flux density [22].

$$T_{cogg}=\frac{l_a r^2}{\mu_0}\int_0^{2\pi}B_r B_\alpha \mathrm{d}\alpha=\frac{\pi l_a r^2}{\mu_0}\sum_k\left(B_{rck}B_{\alpha ck}+B_{rsk}B_{\alpha sk}\right)=\sum_k T_{ck} \tag{6}$$

where l_a is the active axial length, and T_{ck} is the cogging torque component resulting from the k-th order air-gap flux density harmonic.

According to this method, the harmonic content of the radial and tangential air-gap flux density and the cogging torque are related to the $(2n+1)p$-th order.

A method that combines the FE and analytical methods can be used to precisely reflect the effect of each harmonic on the cogging torque. The radial and tangential air-gap flux density components are obtained by the FE model, and then the change in the

cogging torque is analyzed by the Maxwell stress tensor. The contribution of each order flux density harmonic to the cogging torque can be calculated by the FE method at any time in the electric period.

3 SPM motors with various magnetic pole shapes

To verify the theoretical analysis, integer slot and fractional slot motors were established. In this paper, the 12-pole/36-slot motor and 12-pole/18-slot motor are employed for illustration. Although the stator slots of these two models are different, the other parameters are not. The main parameters of the motor are listed in Tab. 1.

Tab. 1 Main parameters of the prototype machines

Parameter	Value
Active length/mm	88
Stator outer diameter/mm	125
Stator inner diameter/mm	80
Rotor inner diameter/mm	67
Magnet thickness/mm	5
Air-gap length/mm	1.5
Pole-arc to pole-pitch ratio	0.83
Magnetization	Parallel
Rated speed/(r/min)	1 000

3.1 Eccentric magnetic poles

The bread-loaf eccentric magnetic pole structure is shown in Fig. 2b. Compared with arc magnets, bread-loaf magnets have a flat bottom, and the thickness of the magnet pole is unevenly distributed. The center of the circle is O. However, when the eccentric design is adopted, the center of the external diameter of the eccentric bread-loaf magnet arc is O_1. The distance between O and O_1, which represents the eccentricity, is h.

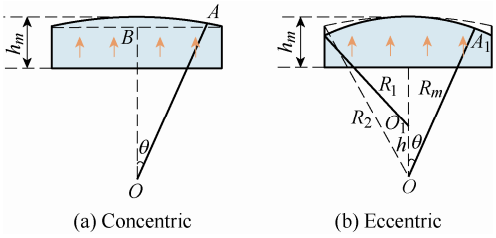

(a) Concentric (b) Eccentric

Fig. 2 Bread-loaf eccentric magnetic pole structure

From the geometrical relationship in Fig. 2, the outer arc radius OA_1 of PM can be expressed as

$$OA_1 = R_m(\theta) = h\cos\theta + \sqrt{R_1^2 - (h\sin\theta)^2} = h\cos\theta + \sqrt{(R_s - g - h)^2 - (h\sin\theta)^2} \quad (7)$$

where g is the length of air gap, h is the eccentricity, and θ is the angle between OA_1 and the center of permanent magnet; the range of θ is $[-\pi\alpha_p/2p, \pi\alpha_p/2p]$. p is the number of pole pairs and α_p is the ratio of the pole-arc to the pole-pitch of the magnets.

According to formula (7), the distribution of the outer radius of the magnet poles with the eccentricity is shown in Fig. 3. It can be seen that the maximum outer radius does not change.

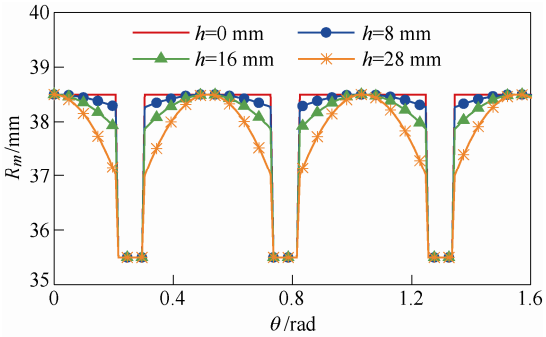

Fig. 3 External radius of magnet poles variation with h

3.2 Sine harmonic compensation

Fig. 4 shows the bread-loaf magnetic poles with sine harmonic compensation. The position of the maximum outer arc radius OA_2 is determined by the value of the third harmonic injected into the magnetic poles shape. Although the outer arc radius for all motors varies, its maximum value, and the PM maximum thickness h_m are maintained. The maximum values of the outer arc radius and PM thickness are 38.5 mm and 5 mm, respectively.

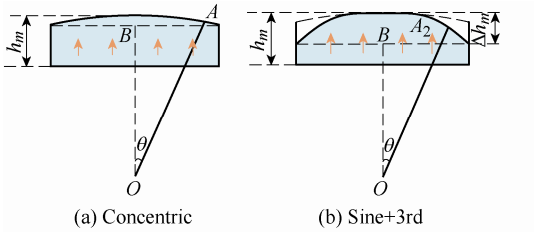

(a) Concentric (b) Sine+3rd

Fig. 4 Bread-loaf magnetic poles with sine harmonic compensation

With the addition of the third harmonic, the PM thickness $\Delta h_m(\theta)$ can be expressed as [15]

$$\Delta h_m(\theta) = m_a[\sin\theta + a_0\sin(3\theta)] \quad (8)$$

where m_a and a_0 are the parameters to be determined,

a_0 is the amplitude of injecting third harmonic, and m_a varies with the value of the injected third harmonic to maintain the same maximum magnet thickness.

The position of the maximum magnet thickness should be first ascertained by determining the relationship between $\Delta h_m(\theta)$ and θ and equating it to zero

$$\frac{\mathrm{d}\Delta h_m(\theta)}{\mathrm{d}(\theta)} = m_a[\cos\theta + 3a_0\cos(3\theta)] = 0 \tag{9}$$

Therefore, the maximum PM thickness occurs at

$$\cos(\theta) = \left(\frac{9a_0 - 1}{12a_0}\right)^{\frac{1}{2}} \tag{10}$$

To have the same maximum magnet thickness as the original magnet shape, $\Delta h_m(\theta)$ should be equal to Δm.

$$m_a = \frac{1}{8a_0}\left(\frac{3a_0 + 1}{12a_0}\right)^{-\frac{3}{2}}\Delta m \tag{11}$$

where Δm is the arc magnet thickness.

The constant + sine + 3rd shaped PM is primarily employed

$$OA_2 = R_m(\theta) = \Delta h_m(\theta) + OB = a\sin(\theta) + b\sin(3\theta) + OB \tag{12}$$

where a and b are constants, whose values can be calculated by formula (11). In this study, the maximum thickness Δm of the arc magnet is 3 mm, the value of a and b are 3.41 and 0.414, respectively.

4 Simulation

Magnetic poles with eccentricity and third harmonic compensation were applied in the 12-pole/36-slot and 12-pole/18-slot motors. The electromagnetic performance of the motor with different magnetic poles shape was analyzed by the FE method. The influence of different magnet pole shapes on motor performance was compared. The rotors of different PM shapes are shown in Fig. 5.

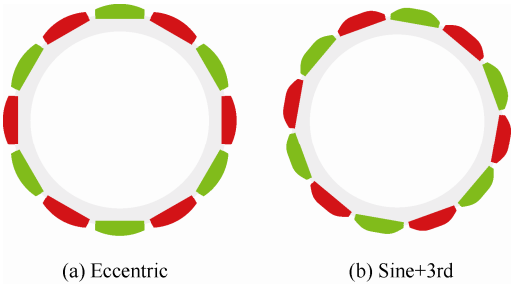

(a) Eccentric (b) Sine+3rd

Fig. 5 Rotor with different magnetic pole shapes

4.1 Eccentric PM poles of the 36-slot and 18-slot motors

We analyzed the eccentricity, open-circuit flux density distribution, and torque.

Fig. 6 shows that the FE predicted fundamental harmonic and total harmonic distortion (THD) of the air-gap flux density for different h of the 12-pole/36-slot motor and the 12-pole/ 18-slot motor

$$\mathrm{THD} = \frac{\sqrt{\sum_{n=2}^{\infty} B_n^{\,2}}}{B_1} \tag{13}$$

where B_n is the amplitude of the air-gap flux density harmonic. B_1 is the fundamental air-gap flux density.

It can be seen that the concentric magnet pole has the highest fundamental, and h = 24 mm has the lowest THD of all the investigated eccentricities. The fundamental value always decreases with an increase in h, while the THD first decreases and then increases. Hence, the optimal h of 24 mm exists for the minimum THD.

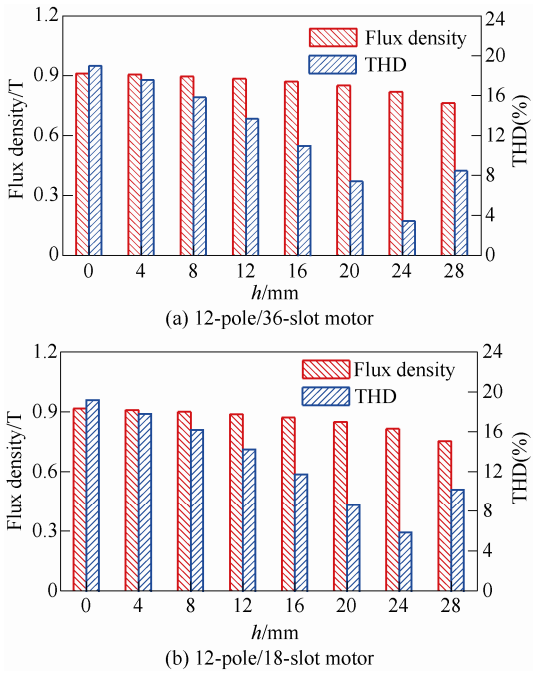

Fig. 6 Variation in the fundamental harmonic and THD of air-gap flux density with different eccentricity

In Fig. 7, the peak cogging torque value and the torque ripple of the 36-slot motor reduce with an increase in h. However, the torque ripple of the 18-slot motor first reduces and then increases, that is, the same magnet shape has different influences on the 36-slot and 18-slot motors.

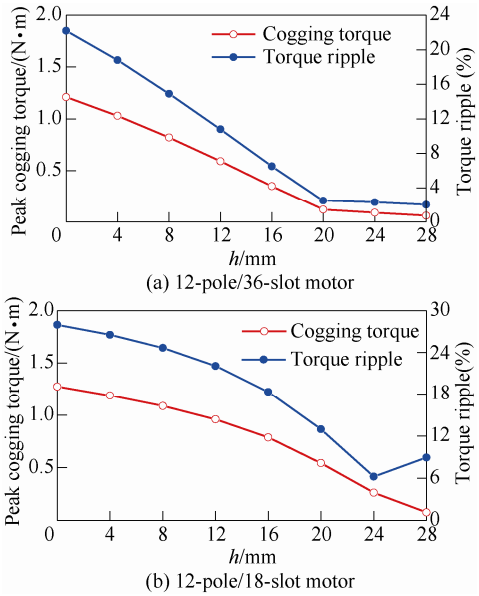

Fig. 7 Influence of eccentricity on torque performance

Fig. 8 shows the cogging torque with/without eccentricity. Compared with the concentric magnet pole, the eccentric magnet pole can significantly reduce the cogging torque in the 36-slot and 18-slot motors. At the same eccentricity, the cogging torque reduction trend of the 18-slot motor is significantly lower than that of the 36-slot motor.

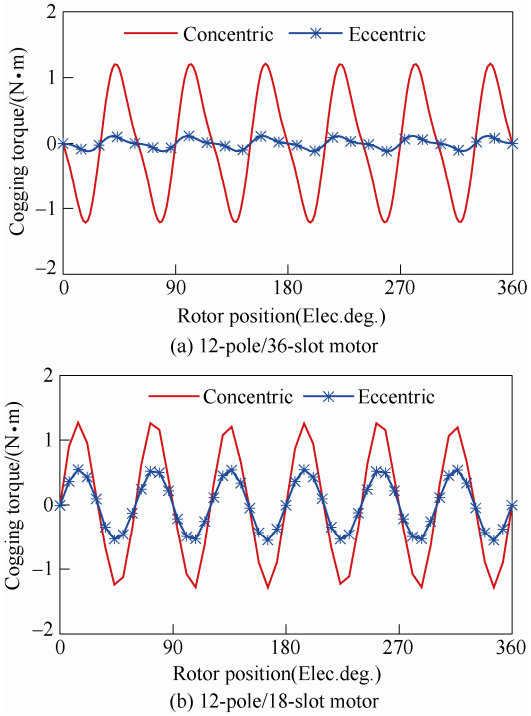

Fig. 8 Cogging torque with/without eccentricity

To determine why the eccentric magnet pole resulted in a smaller cogging torque, the air-gap flux density and torque contribution of the magnetic flux harmonics to the cogging torque were analyzed.

The rotor positions of 45 electrical degrees and 22 electrical degrees were analyzed because the respective peaks of the cogging torque waveforms of the 36-slot and 18-slot motors appear at these rotor positions. For the 12-pole/36-slot motor, the influence of the eccentric magnet pole on the air-gap flux density is shown in Fig. 9. According to formulas (1)-(6), the harmonic amplitude is determined by the 6-th, 18-th, 30-th, ⋯ harmonic orders, and the harmonics of other orders do not exist. As shown, the FE method results are consistent with those of the analytical method. In Fig. 9a, the air-gap flux density becomes more regular after eccentricity. A component of air-gap flux density harmonic with different eccentricity is shown in Fig. 9b. Compared with those of the concentric magnetic poles, the amplitudes of the air-gap flux density harmonics of the eccentric magnetic poles are lower. Moreover, the additional field harmonics cannot be produced by the eccentric magnet pole.

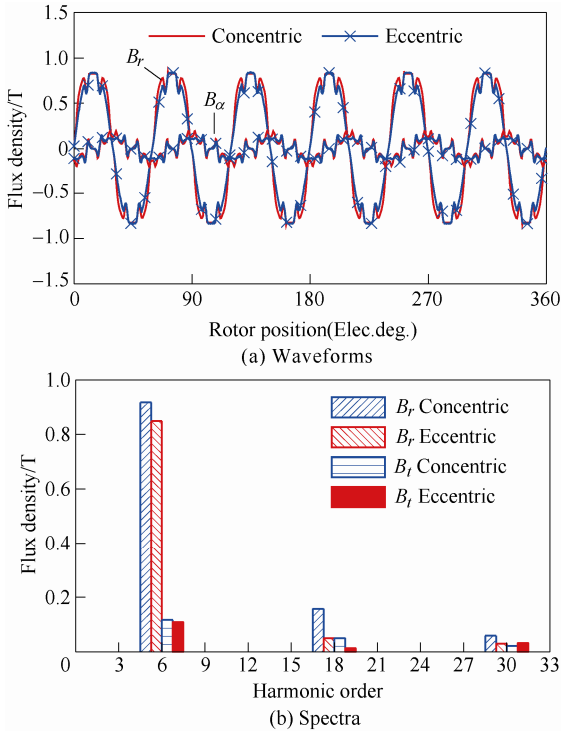

Fig. 9 Air-gap flux density of the 12-pole/36-slot motor with/without eccentricity

For the 12-pole/18-slot motor, the influence of the eccentric magnet pole on the air-gap flux density is shown in Fig. 10. In Fig. 10b, compared with that of the 12-pole/36-slot motor, the air-gap flux density of the 12-pole/18-slot motor contains more field harmonics, e.g., the 6-th, 12-th, 18-th, 24-th, and the 30-th field harmonics. In theory, the air-gap magnetic density is related to the $(2n + 1)\ p$ = 6-th, 18-th, ⋯

These harmonics are determined by the magnetization of magnets. The 24-th harmonic is due to the stator slotting effect. Compared with other harmonics, the 12-th and 24-th field harmonics are insignificant.

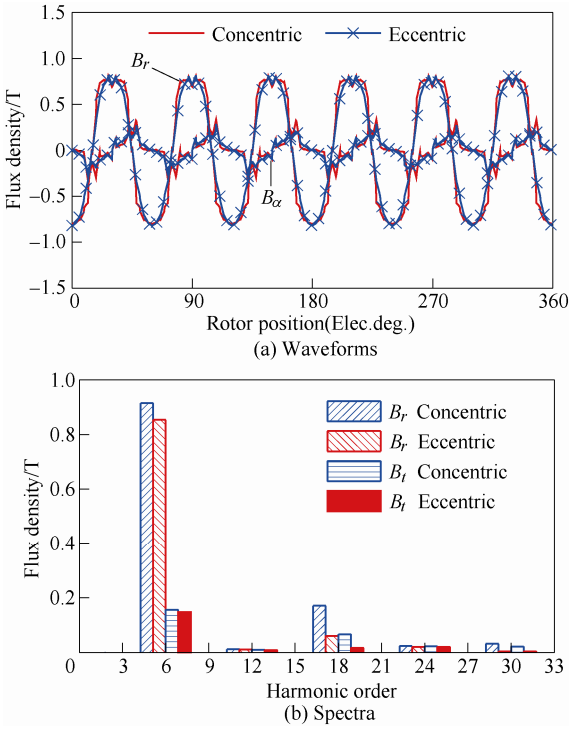

Fig. 10 Air-gap flux density of the 12-pole/18-slot motor with/without eccentricity

The contribution of each flux density harmonic to the cogging torque is shown in Fig. 11. From Fig. 11a, it can be seen that the cogging torque can be produced with a concentric magnet pole by the 6-th, 18-th, 30-th and 42-th field harmonics. Furthermore, the 30-th harmonic makes the greatest contribution to the cogging torque. When the magnetic pole is eccentric, the amplitudes of the cogging torques produced by the 6-th, 18-th, 30-th and 42-th field harmonics decrease. The 6-th and 30-th harmonics have a negative effect on the production of the cogging torque. The same analysis can be applied to the 18-slot motor. It can be seen that the additional harmonics cannot be produced by the eccentric magnetic pole. The FE method analysis shows that the cogging torque is produced by the $(2n+1)p$-th harmonic, and the cogging torque can be reduced by the eccentric magnet pole.

Figs. 12 and 13 show the instant cogging torque contribution of individual field harmonics in the 36- and 18-slot motors. The cogging torque produced by the k-th magnetic field harmonic can be calculated by formula (6) in the entire electric period. For the 12-pole/36-slot motor, with the concentric magnet pole, the total cogging torque is mainly determined by the 6-th, 18-th, 30-th, and 42-th order field harmonics as shown in Fig. 12a. It can be seen that the component of the cogging torque produced by the 30-th harmonic is more than that produced by other orders. Again, for

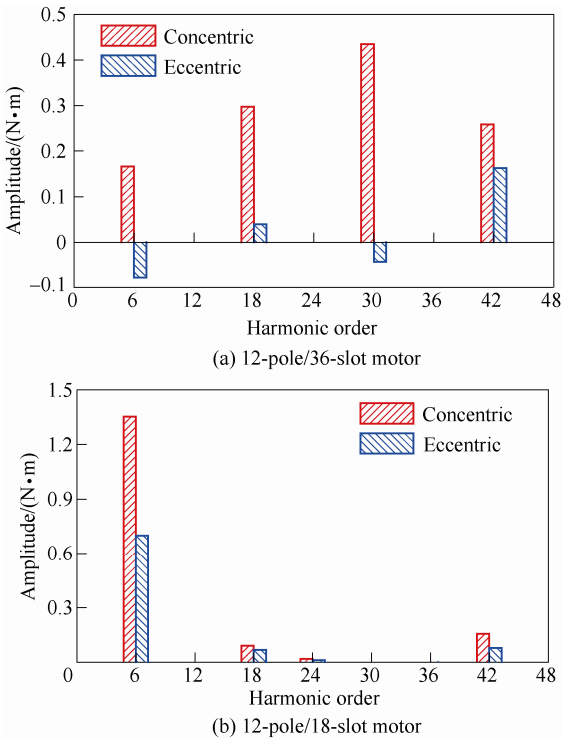

Fig. 11 Torque contribution of each air-gap flux density harmonic to the cogging torque

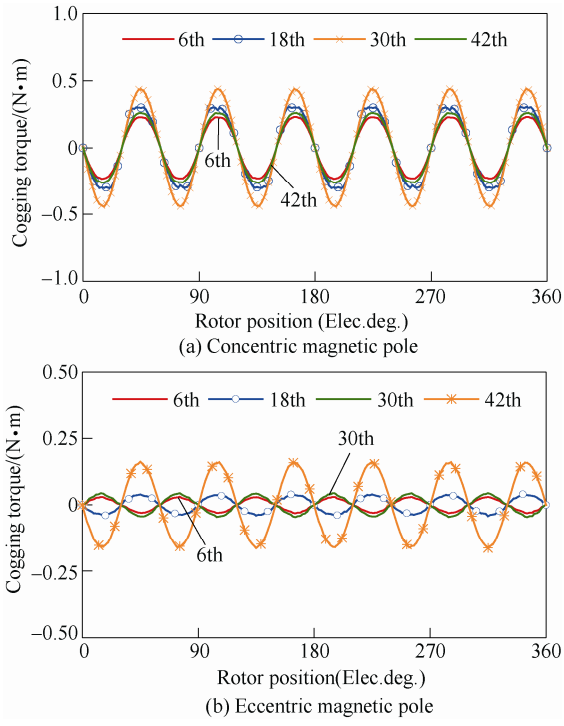

Fig. 12 Instant cogging torque contribution of individual field harmonics of the 12-pole/36-slot motor

the same motor, the magnet pole eccentricity results in a significant reduction in the cogging torque amplitude produced by individual field harmonics. The 42-th harmonic produces the largest cogging torque components, while the 6-th and the 30-th cogging torque harmonics have a negative effect on the total cogging torque. In other words, the cogging torque due to the eccentric magnet pole originates from the 42-th harmonic in the 12-pole/36-slot motor.

For the 12-pole/18-slot motor, the 6-th harmonic is the main source of the cogging torque in Fig. 13a. Compared with the concentric magnet pole, the eccentric magnet pole results in a reduction in the amplitude of the cogging torque produced by individual field harmonics.

The eccentric magnet pole reduces the cogging torque in both motors. However, the cogging torque reduction of the integer slot motor has a greater effect at the same eccentricity. The magnetic pole eccentricities in the 12-pole/36-slot and the 12-pole/18-slot motors hardly affect the harmonic contents of the cogging torque; however, they slightly change the harmonic magnitude. Under the same degree of eccentricity, the reduction in the cogging torque in the 36-slot motor is greater than that in the 18-slot motor. This is because the eccentricity of magnetic poles can lead to cogging torque harmonics in the 36-slot motor that produce negative effects.

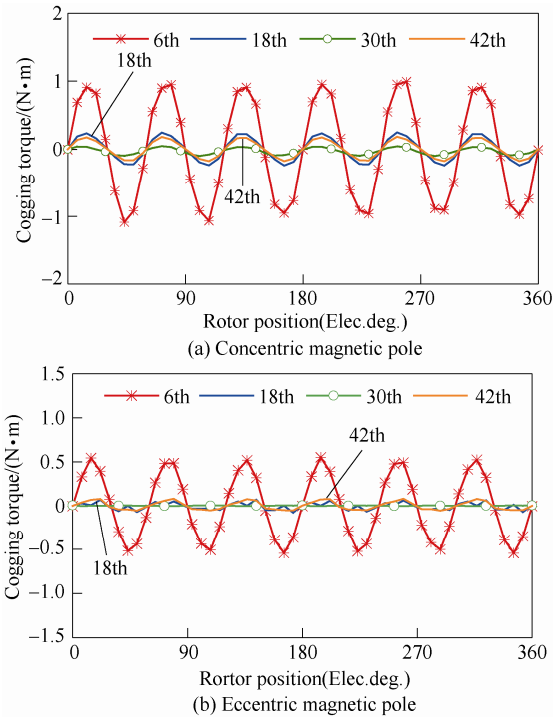

Fig. 13 Instant cogging torque contribution of individual field harmonic of the 12-pole/18-slot motor

Fig. 14 shows the variation in the torque with eccentricity of the magnet pole. The cogging torque, the average torque, the torque ripple, and the torque loss of the 36-slot and 18-slot motors with various magnet shapes are compared in Tab. 2. Compared with those of the concentric magnet pole, the cogging torque and the average torque of the 36-slot and 18-slot motors with eccentric magnetic poles decrease. The torque ripple of the 18-slot motor reduced from 28.0 % to 13.0% and the torque ripple of the 36-slot motor decreased from 22.2% to 2.5%. The reduction extent of the torque ripple in the 18-slot motor is larger than that of the 36-slot motor when they have the same magnetic pole shape. The torque losses of the 36- and 18-slot motors are 7.8% and 5.8%, respectively.

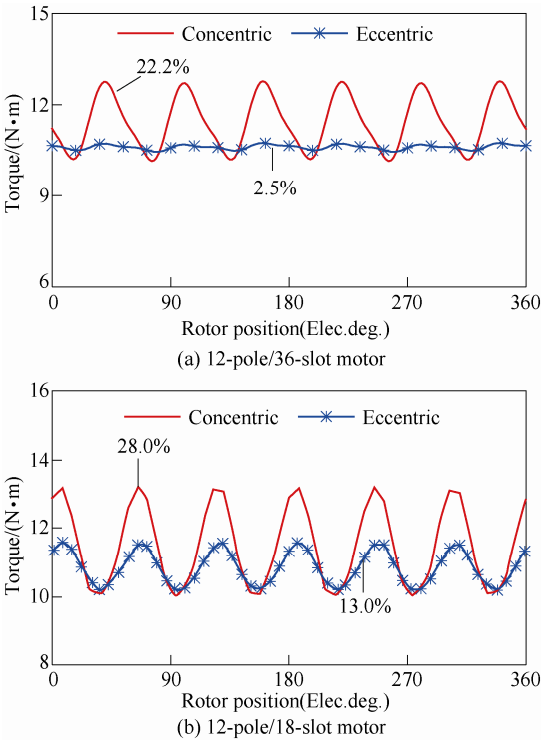

Fig. 14 Torque with/without eccentricity

Tab. 2 Torque analysis

Parameter	Concentric		Eccentric	
2p/Q	12/36	12/18	12/36	12/18
Peak cogging torque/nm	1.21	1.27	0.11	0.54
Torque/nm	11.5	11.5	10.6	10.83
Torque ripple(%)	22.2	28.0	2.5	13.0
Torque loss(%)	—	—	7.8	5.8

4.2 PM shape with third harmonic of the 36-slot and 18-slot motors

The influence of eccentric magnetic poles on the

cogging torque has been analyzed. It was found that magnetic pole eccentricity improves the torque performance of the 36-slot motor. In this section, the electromagnetic performance of the third harmonic injected into the magnetic pole shape is analyzed by the same analysis method.

The variation in the cogging torque with rotor position is shown in Fig. 15. For the 12-pole/36-slot motor, the maximum value of the cogging torque with sine harmonic compensation is 1 nm. Compared with the original cogging torque, the maximum cogging torque value is decreased by 0.21 nm in Fig. 15a. However, for the 12-pole/18-slot motor, the maximum value of the cogging torque with sine harmonic compensation is 0.28 nm. These findings indicate that the sine harmonic compensation reduces the cogging torque of the fractional slot motor.

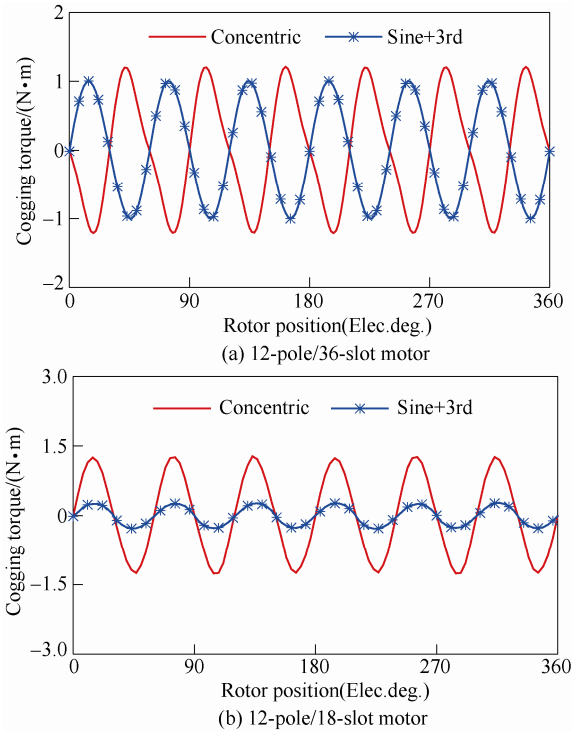

Fig. 15 Variation in the cogging torque with rotor position

Fig. 16 shows the contribution of each air-gap flux density harmonic to the cogging torque, while the instant cogging torque contribution of individual field harmonics is shown in Fig.17. Figs. 16 and 17 are studied to analyze the source of the cogging torque.

The sources of the cogging torque with sine harmonic compensation are the 6-th, 18-th, 30-th, and 42-th field harmonics. For the 12-pole/36-slot motor, the cogging torque amplitudes produced by the 6th, 18-th, and 42-th field harmonics are reduced. The cogging torque amplitude caused by the 30-th field harmonic increases, however. The instant cogging torque contribution of individual field harmonics is shown in Fig. 17a. Thus, it can be concluded that the 30-th harmonic is the main source of the cogging torque.

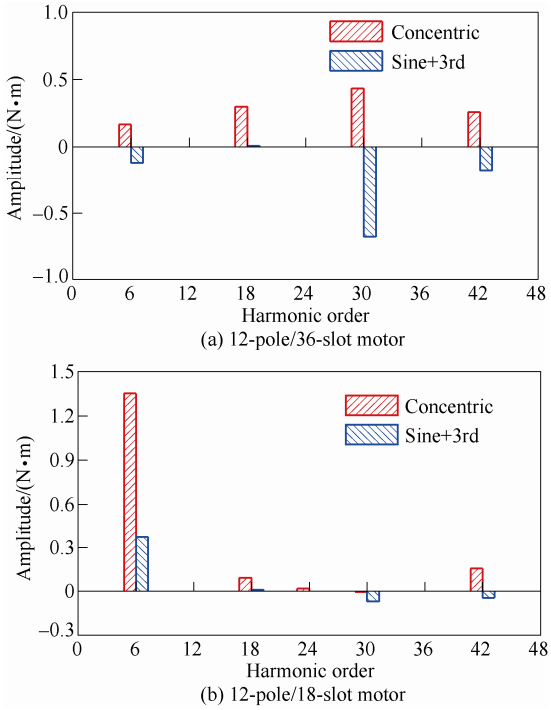

Fig. 16 Torque contribution of each air-gap flux density harmonic to the cogging torque

For the 12-pole/18-slot motor, the main source of the original cogging torque is the 6-th field harmonic, with other field harmonics making little contribution to the cogging torque, as shown in Fig. 16b. Because of the sine harmonic compensation in the magnetic poles, the amplitude of the cogging torque produced by the 6-th, 18-th, and 42-th field harmonics decrease. The cogging torque amplitude caused by the 30-th harmonic increases, as shown in Fig. 17b. The total cogging torque value reduces because the amplitude of the cogging torque produced by the 6-th field harmonic decreases, and the 42-th field harmonic has a negative effect on cogging torque production.

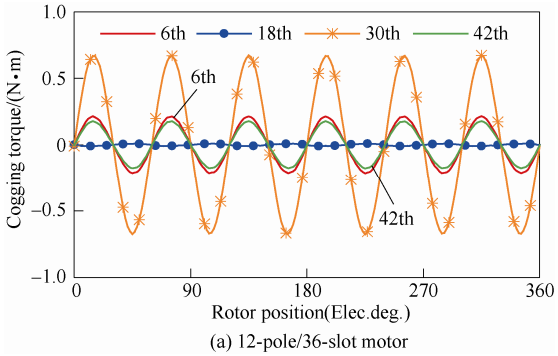

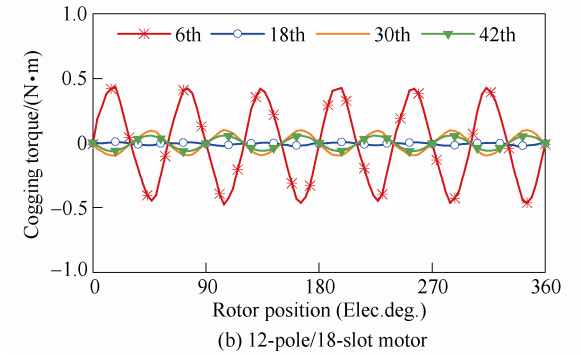

(b) 12-pole/18-slot motor

Fig. 17 Instant cogging torque contribution of individual field harmonics

The variation in the torque with rotor position is shown in Fig. 18. The peak cogging torque, torque, and torque ripple of different motors with the same rotor structure are compared in Tab. 3. For the 12-pole/36-slot motor, when the third harmonic is injected into the magnetic pole, the peak value of the cogging torque and the torque ripple decrease. For the 12-pole/18-slot motor, the peak cogging torque and the torque ripple also decrease. The average torques in the 36- and 18-slot motors decrease because the PM volumes reduce. According to Tabs. 2 and 3, the eccentric magnetic pole has a significant effect on the reduction in the cogging torques and torque ripples of both motors; thus, the magnetic pole with sine harmonic compensation is suitable for use in the fractional slot motor.

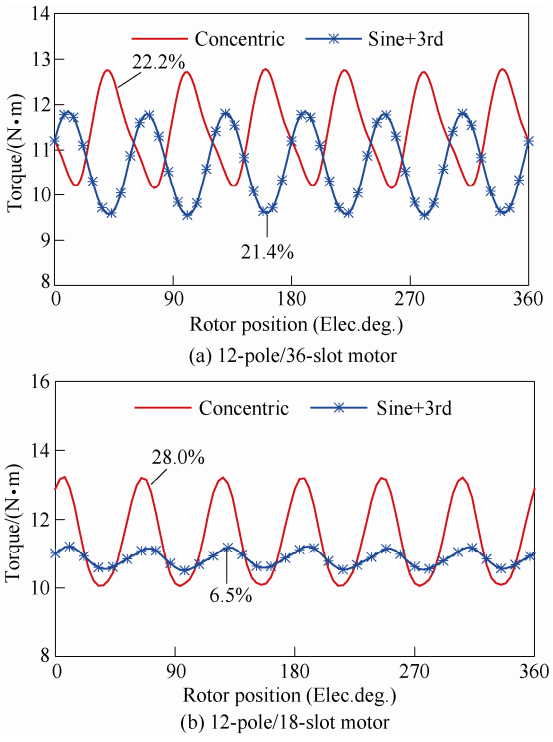

(a) 12-pole/36-slot motor

(b) 12-pole/18-slot motor

Fig. 18 Variation in torque with rotor position

Tab. 3 Torque analysis

Parameter	Concentric		Sine+3rd	
2p/Q	12/36	12/18	12/36	12/18
Peak cogging torque/nm	1.21	1.27	1.00	0.28
Torque/nm	11.5	11.5	10.66	10.85
Torque ripple(%)	22.2	28.0	21.4	6.5
Torque loss(%)	—	—	7.3	5.7

5 Experimental verification

The designed 12-pole/36-slot motor was built and tested to verify the theoretical analysis. The prototype is shown in Fig. 19, and the experimental platform is shown in Fig. 20. Fig. 21 shows the measured and FE predicted three-phase no-load back electromotive forces (EMFs). Comparing Figs. 21a and 21b, it can be seen that the measured back-EMF is consistent with the FE predicted back-EMF. The design of the eccentric magnet pole makes the no-load back-EMF more sinusoidal.

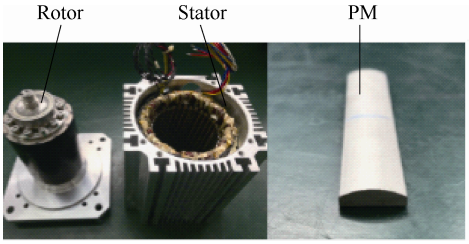

Fig. 19 Prototype

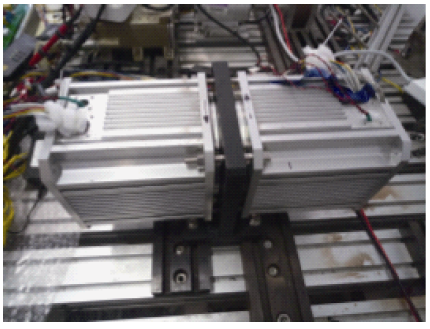

Fig. 20 Experimental platform

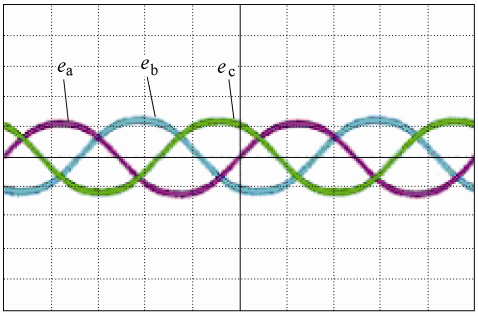

(a) Measured ones(2 ms/div,100 V/div)

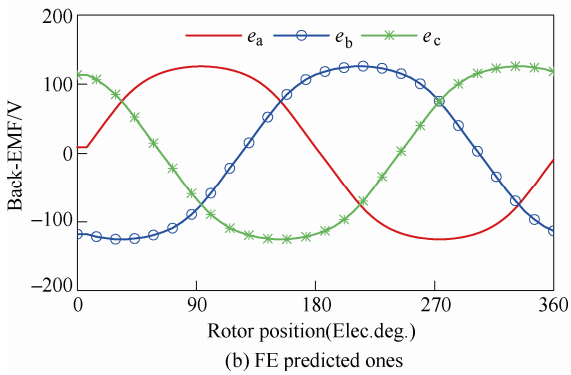

(b) FE predicted ones

Fig. 21 Three-phase no-load back-EMFs

6 Conclusions

In this study, we investigated the influence of a bread-loaf shaped magnet pole on the cogging torque of PM motors. The analysis revealed that the weakening of the $(2n + 1)$ p-th harmonic amplitude of the air-gap flux density is the main reason for the reduction in the cogging torque. The design of the eccentric magnetic pole leads some field harmonics have negative effects to produce the cogging torque. With an increase in h, the cogging torque decreases. Compared with those of the fractional slot motor, the cogging torque and torque ripple of the integer slot motor can be more effectively reduced with the same eccentric magnet pole. The PM shape with sine harmonic compensation can reduce the cogging torque and torque ripple in the fractional slot motor, however, it has a small effect on reducing the cogging torque and torque ripple in the integer slot motor under the same sine harmonic compensation. The FE simulation and experiment results reveal that the design of an eccentric magnetic pole makes the no-load back-EMF more sinusoidal and can effectively weaken the cogging torque and reduce the torque ripple.

References

[1] C Ma, Q Li, L Deng, et al. A novel sound quality evaluation method of the diagnosis of abnormal noise in interior permanent-magnet synchronous motors for electric vehicles. *IEEE Trans. Ind. Electron*., 2017, 64(5): 3883-3891.

[2] M Cheng, L Sun, G Buja, et al. Advanced electrical machines and machine-based systems for electric and hybrid vehicles. *Energies*, 2015, 8(9): 9541-9564.

[3] S Zhu, Y Hu, C Liu, et al. Iron loss and efficiency analysis of interior pm machines for electric vehicle applications. *IEEE Trans. Ind. Electron*., 2018, 65(1): 114-124.

[4] S J Rind, Y X Ren, Y H Hu, et al. Configurations and control of traction motors for electric vehicles: A review. *Chinese Journal of Electrical Engineering*, 2017, 3(3): 1-17.

[5] M Cheng, M H Tong. Development status and trend of electric vehicles in China. *Chinese Journal of Electrical Engineering*, 2017, 3(2): 1-13.

[6] J K Si, S Z Zhao, L F Zhang, et al. The characteristics analysis and cogging torque optimization of a surface-interior permanent magnet synchronous motor, *Chinese Journal of Electrical Engineering*, 2018, 4(4): 41-47.

[7] X Zhu, W Hua, Z Wu, et al. Analytical approach for cogging torque reduction in flux-switching permanent magnet machines based on magneto motive force-permeance model. *IEEE Trans. Ind. Electron.*, 2018, 65(3): 1965-1979.

[8] K Wang, Y P Liang, D M Wang, et al. Cogging torque reduction by eccentric structure of teeth in external rotor permanent magnet synchronous motors. *IET Electric Power Appl.*, 2019, 13(3): 57-63.

[9] I Petrov, P Ponomarev, Y Alexandrova, et al. Unequal teeth widths for torque ripple reduction in permanent magnet synchronous machines with fractional-slot non-overlapping windings. *IEEE Trans. Magn.*, 2015, 51(2): 1-9.

[10] G J Li, Z Q Zhu, M Foster, et al. Comparative studies of modular and unequal tooth PM machines either with or without tooth tips. *IEEE Trans. Magn*., 2014, 50(7): 1-10.

[11] D K Kim, Y U Park, J H Cho. Cogging torque reduction of single-phase brushless DC motor with a tapered air-gap using optimizing notch size and position. *IEEE Trans. Ind. Appl*., 2015, 51(6): 2447-2453.

[12] G J Li, B Ren, Z Q Zhu, et al. Cogging torque mitigation of modular permanent magnet machines. *IEEE Trans. Magn*., 2016, 52(1): 1-10.

[13] Z T Du, T Lipo. Efficient utilization of rare earth permanent-magnet materials and torque ripple reduction in interior permanent-magnet machines. *IEEE Trans. Ind. Appl*., 2017, 53(4): 3485-3495.

[14] L B Jing, Z H Luo, R H Qu, et al. Investigation of a surface PM machine with segmented-eccentric magnet poles. *IEEE Trans. Appl. Super*., 2018, 28(3): 1-5.

[15] K Wang, Z Q Zhu, G Ombach. Torque enhancement of surface-mounted permanent magnet machine using third-order harmonic. *IEEE Trans. Magn*., 2014, 50(3): 1-10.

[16] Z T Du, T Lipo. High torque density and low torque ripple shaped-magnet machines using sinusoidal plus third

harmonic shaped magnets. *IEEE Trans. Ind. Appl*., 2019, 55(3): 2601-2610.

[17] S A Saied, K Abbaszadeh, A Tenconi, et al. New approach to cogging torque simulation using numerical functions. *IEEE Trans. Ind. Appl.*, 2014, 50(4): 2420-2426.

[18] S Ruangsinchaiwanich, Z Q Zhu, D Howe. Influence of magnet shape on cogging torque and back-emf waveform in permanent magnet machines. *International Conference on Electrical Machines and Systems*, *IEEE*, 2005.

[19] T Wegiel. Cogging torque analysis based on energy approach in surface-mounted PM machines. *Proc. Int. Symp. Electr. Mach*., 2017: 1-6.

[20] F Ebadi1, M Mardaneh, A Rahideh, et al. Analytical energy-based approaches for cogging torque calculation in surface-mounted PM motors. *IEEE Trans. Magn.*, 2019, 55(5): 1-10.

[21] Z Q Zhu, L J Wu, Z P Xia. An accurate subdomain model for magnetic field computation in slotted surface-mounted permanent-magnet machines. *IEEE Trans. Magn*., 2010, 46(4): 1100-1115.

[22] Z F Chen, C L Xia, Q Geng, et al. Modeling and analyzing of surface-mounted permanent-magnet synchronous machines with optimized magnetic pole shape. *IEEE Trans. Magn*., 2014, 50(11): 1100-1115.

[23] Y Zhou, H S Li, G W Meng, et al. Analytical calculation of magnetic field and cogging torque in surface-mounted permanent-magnet machines accounting for any eccentric rotor shape. *IEEE Trans. Ind. Electron*., 2015, 62(6): 3438-3446.

[24] Yu Zeng, Ming Cheng, Guohai Liu, et al. Effects of magnet shape on torque capability of surface-mounted permanent magnet machine for servo applications. *IEEE Trans. Ind. Electron*., 2019, PP(99):1-1. DOI:10.1109/TIE.2019.2910025.

Min Zhou received the B.S. degree in electronic science and technology from Yancheng Institute of Technology, Yancheng, China, in 2017, and she is currently working toward the M.Sc. degree in power engineering and engineering thermophysics. Her current research interests include computation of electromagnetic fields for permanent-magnet machine and electric machine designs.

Xinxing Zhang received the B.S. and M.S. degrees from Jiangsu University, Zhenjiang, China, in 2015 and 2018, respectively. She is currently working at Jingjiang College, Jiangsu University. Her current research interests include computation of electromagnetic fields for permanent-magnet motor and motor design.

Wenxiang Zhao (M'08-SM'14) received the B.S. and M.S. degrees from Jiangsu University, Zhenjiang, China, in 1999 and 2003, respectively, and the Ph.D. degree from Southeast University, Nanjing, China, in 2010, all in electrical engineering.

He has been with Jiangsu University since 2003, where he is currently a Professor with the School of Electrical Information Engineering. From 2008 to 2009, he was a Research Assistant with the Department of Electrical and Electronic Engineering, University of Hong Kong, Hong Kong. From 2013 to 2014, he was a Visiting Professor with the Department of Electronic and Electrical Engineering, University of Sheffield, Sheffield, U.K. His current research interests include electric machine design, modeling, fault analysis, and intelligent control. He has authored and co-authored over 130 technical papers in these areas.

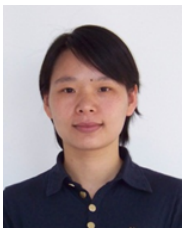

Jinghua Ji received the B.S., M.S., and Ph.D. degrees in electrical engineering from Jiangsu University, Zhenjiang, China, in 2000, 2003, and 2009 respectively. Since 2000, she has been with the School of Electrical and Information Engineering, Jiangsu University, where she is currently a Professor. From 2013 to 2014, she was a Visiting Scholar with the Department of Electronic and Electrical Engineering, University of Sheffield, Sheffield, U.K.

Her areas of interest include motor design and electromagnetic field computation. She has authored and co-authored over 50 technical papers in these areas.

Jingning Hu received the B.S. degree in hydraulic machinery from Tsinghua University, Beijing, China, in 1984. From 1984 to 2004, he was in the industrial pump branch of Hefei General Machinery Research Institute, Ministry of machinery. He has been with the Research Center of Fluid Machinery Engineering and Technology, Jiangsu University since 2004, where he is currently a Professor. His current research interests include research and development of centrifugal pump products and localization of major equipment.